Volume 59
Number 41
21 May 2023
Pages 6099–6260

ChemComm

Chemical Communications

rsc.li/chemcomm

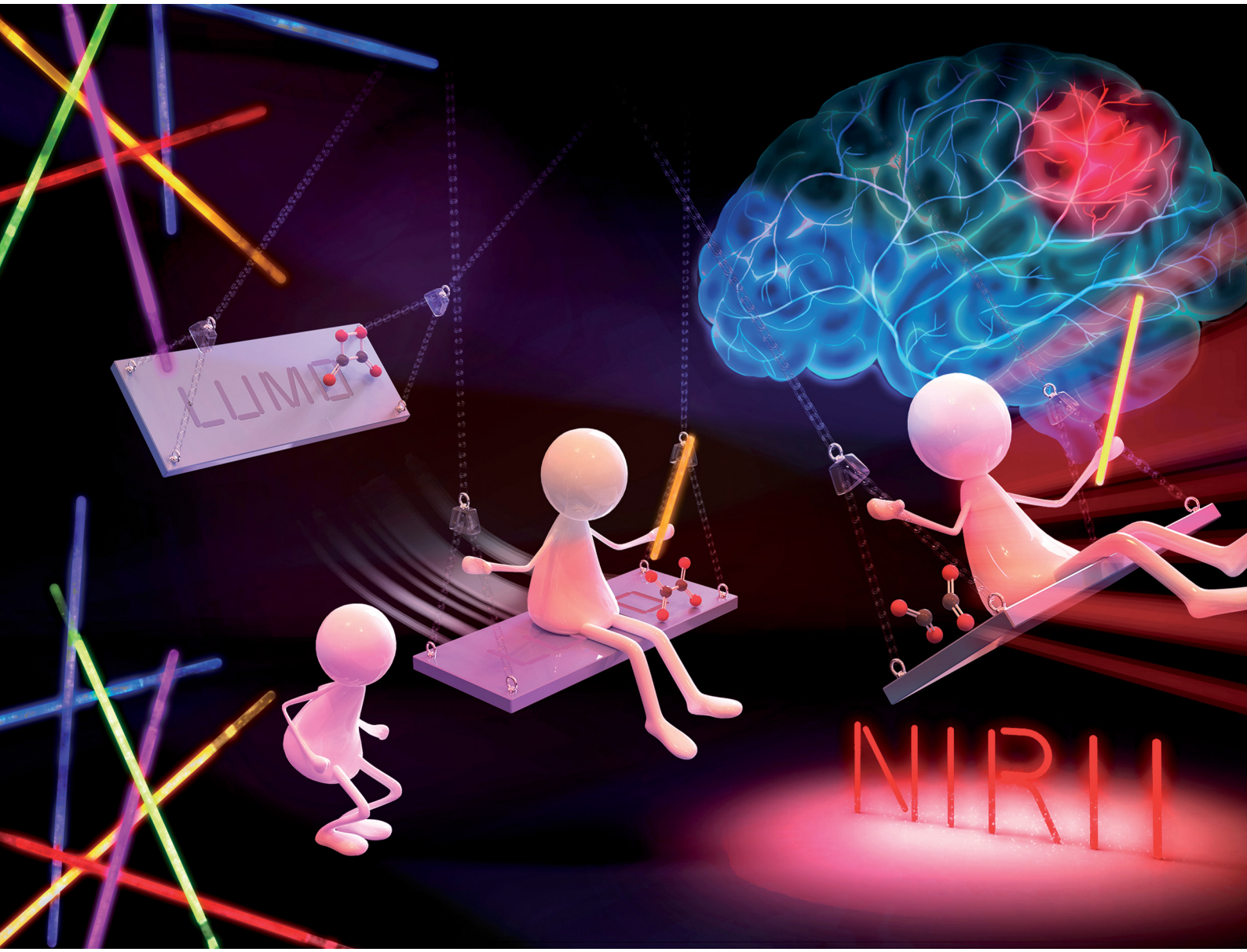

ISSN 1359-7345

ROYAL SOCIETY OF CHEMISTRY

COMMUNICATION

Huageng Liang, Jie Ding, Xiaoping Zhang, Qinchao Sun *et al.*
Single-dye NIR-II chemiluminescence system for H_2O_2 imaging

ChemComm

COMMUNICATION

View Article Online
View Journal | View Issue

Cite this: *Chem. Commun.*, 2023, 59, 6171

Received 3rd December 2022,
Accepted 20th March 2023

DOI: 10.1039/d2cc06592d

rsc.li/chemcomm

Single-dye NIR-II chemiluminescence system for H_2O_2 imaging†

Zong Chang,‡[a] Chenchen Liu,‡[ab] Like Guo,[c] Bingxin Shu,[a] Huageng Liang, *[b] Jie Ding, *[c] Xiaoping Zhang*[b] and Qinchao Sun*[a]

An efficient single-dye NIR-II CL system was proposed for the first time with the longest emission peak around 1000 nm. Biocompatible CL nanoparticles were developed and a surprising CL intensity enhancement was found in the presence of the BASZn nanoenzyme by about three orders of magnitude. Such an NIR-II CL system was demonstrated for glucose sensing, tumor therapy and *in vivo* H_2O_2 imaging. *Via* theoretical and experimental analyses, a novel electron transfer model was established for such a chemiluminescence system rather than the generally considered $HOMO_{Dye}$–$LUMO_{DOD}$ model. These findings provide useful guidelines for designing efficient single-dye NIR-II CL systems.

NIR-II photons have been demonstrated to dramatically improve the *in vivo* imaging resolution in heavily scattering tissue environments, for instance the NIR-II photoluminescence imaging of mouse intact brain vessels.[1–4] In comparison to photoluminescence (PL), chemiluminescence (CL) imaging is considered to provide better signal to noise ratio as no excitation beam-related background noise is involved.[5–10] One of the most famous CL systems is the oxalate ester (CPPO) and dye involved, H_2O_2 triggered system, which provides the ideal approach to *in vivo* image the H_2O_2 metabolic status in tumors, inflamed tissues and the liver during drug clearance.[11–17] Thanks to the generation of energetic intermediate DOD, such a system is capable of transferring the chemical energy to excited electronic energy of various dyes *via* two-step electron transfer (eT), Scheme 1(a).[12] Most recent studies have assigned the CL efficiency limiting step as the electron transfer from the $HOMO_{Dye}$ to the $LUMO_{DOD}$ (Scheme 1(b)).[13,14] According to such an argument, a multi-dye energy transfer system was necessary for realizing the NIR CL (Scheme 1(a)), especially for NIR-II, considering the high energy gap of $LUMO_{DOD}$–$HOMO_{Dye}$.[13,15] In the last two years, multi-dye NIR-II CL systems with luminescence maximum around 950 nm were reported for H_2O_2-induced tissue inflammation imaging.[13,15,16] However, such a multi-dye energy transfer process might make the CL system more complicated and less efficient.

Cyanine dyes have been intensively studied not only for biological research but in clinical medicine as well,[17,18] due to the excellent photo-properties.[2] For instance, ICG is a unique FDA approved fluorophore with an emission band beyond 800 nm.[18] The electronic transition energy of cyanine dyes could be feasibly tuned from visible to NIR due to the unique electronic structure of the polymethine bonds.[2] NIR-II emission cyanine dyes have been studied for the past decade as excellent fluorescence probes for photoluminescence imaging.[17,19–21]

Herein, the first efficient single-dye NIR-II CL system with the longest emission peak over 1000 nm was realized other than resorting to the complicated multi-dye energy transfer strategy.

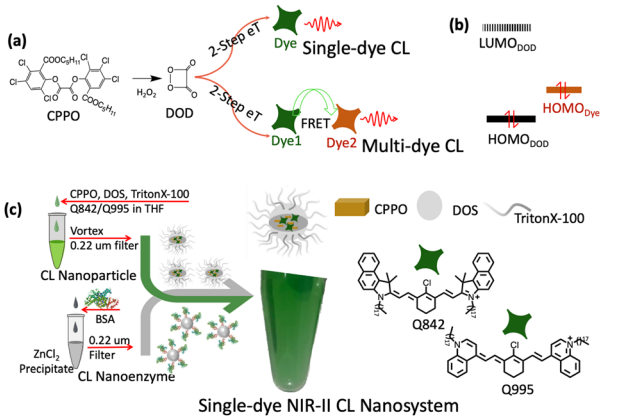

Scheme 1 (a) The CL mechanism of single-dye CL and multi-dye CL. (b) The frontier orbitals of DOD and the dye. (c) The preparation of the single-dye NIR-II CL nanosystem of cyanine dye Q995 and Q842.

[a] *Guangdong Provincial Key Laboratory of Biomedical Optical Imaging Technology and Center for Biomedical Optics and Molecular Imaging, Shenzhen Institute of Advanced Technology, CAS, Shenzhen 518055, China. E-mail: qchao.sun@siat.ac.cn*

[b] *Department of Urology, Huazhong University of Science and Technology, Wuhan 430022, China. E-mail: wleonard19800318@hust.edu.cn, xzhang@hust.edu.cn*

[c] *Green Catalysis Center, College of Chemistry, Zhengzhou University, Zhengzhou 450000, China. E-mail: jieding@zzu.edu.cn*

† Electronic supplementary information (ESI) available. See DOI: https://doi.org/10.1039/d2cc06592d

‡ Z. C., C. L. contributed equally.

A BSAZn-based nanoenzyme was developed to dramatically enhance the NIR-II CL nanosystem for about three orders of magnitude. Such a single-dye NIR-II CL system was demonstrated for glucose sensing, tumor therapy and *in vivo* H_2O_2 imaging. Furthermore, we found that the NIR-II chemiluminescence intensity was mainly dominated by the emission QY of the dye, rather than the usually considered energy gap of $LUMO_{DOD}$–$HOMO_{Dye}$. Frontier molecular orbitals were analyzed to reach an electron transfer swing model for designing novel efficient NIR-II CL systems.

An outstanding NIR-II CL could be realized *via* two kinds of cyanine dye Q995 and Q842, respectively (Fig. S1 and S2, ESI†). According to the typical molecular structure of cyanine dyes, the photophysical properties could be substantially adjusted by altering the length of the polymethine linker and gently varied by the electronic properties of the heterocyclic groups.[2] However, a surprisingly large red shifted fluorescence was realized for Q995 of about 150 nm (Fig. 1(a) and Table 1) with the same polymethine linker as Q842 (Fig. S1, ESI†). It might come from the extended length of the polymethine linker for Q995 *via* the quinoline group, Fig. S1 (ESI†). Though the emission maximum of Q842 is in the NIR-I region, the emission intensity beyond 1000 nm was found to be similar to that of Q995 and much larger than that of IR26 (commercial NIR-II dye), Fig. 1(b) and Table 1. The excellent photophysical properties of Q995 and Q842 render a bright CL in NIR-II, Fig. S2 (ESI†). Fig. 1(c) shows the CL spectra of Q995 and Q842 in THF solution, which are of similar emission maximum as the corresponding photoluminescence.

The biocompatible single-dye NIR-II CL nanoparticle was prepared, as shown in Scheme 1(c). Briefly, the CPPO, DOS, TrionX-100 and corresponding dye were dissolved in THF and then dropwise mixed with water under vortexing. The hydrodynamic diameter of the prepared nanoparticles was around 50 nm, Fig. S3 (ESI†). To increase the solubility in THF and the miscibility with DOS for the preparation of nanoparticles, a long alkyl chain was introduced to Q995 and Q842. We surprisingly found that the CL intensity of the CL nanoparticles could be dramatically enhanced by the BSAZn nanocomplexes (Fig. 1(d)–(g)), which were prepared by dissolving the precipitate from the $ZnCl_2$ aqueous solution into BSA solution (details in the ESI†). For Q842 CL nanoparticles, the CL intensity was about thousands-fold enhanced in the presence of BSAZn for observation beyond 900 nm, and about 100-fold beyond 1000 nm, Fig. 1(d) and (f). No observable CL was found for the THF solution and in the absence of the BSAZn under such low H_2O_2 concentration and short exposure time. For Q995 CL nanoparticles, enhancement was also observed in the presence of BSAZn, Fig. 1(e) and (f). A similar enhancement effect was observed from ZnO nanoparticles and the corresponding BSA nanocomplexes, Fig. S4 (ESI†). The XRD measurements indicate the presence of ZnO for the precipitate ($ZnCl_2$ aqueous solution) and BSAZn, Fig. S5 (ESI†). In contrast, no observable enhancement has been recorded for the Zn^{2+} ion solution, as shown in Fig. S4 (ESI†). The BSAZn might work as a kind of nanoenzyme to facilitate the decomposition of H_2O_2.[22a]

The CL kinetics of the Q842 nanoparticles was depicted in Fig. 1(g). We may find that the CL intensity decays exponentially with a lifetime of about 180 s. The addition of fresh Q842 nanoparticles was found to restore the CL intensity to a similar level as at the beginning and the morphology of the BSAZn nanoenzyme remained stable throughout the CL reaction, Fig. S11 (ESI†). These observations indicate that the BSAZn exhibits mild catalysis that is quite stable in the system. The Q842 NIR-II CL nanosystem exhibits remarkable sensitivity to H_2O_2, as illustrated in Fig. 1(h) and (i). At high Q842 concentration, the linear response detection limit was found to be as low as 5 μM of H_2O_2, Fig. S7 (ESI†). Moreover, the CL nanosystem demonstrates excellent selectivity towards H_2O_2, as observed in Fig. S12 (ESI†).[22b,c] Interestingly, we also found that the CPPO would spontaneously decompose in the CL nanoparticles at 37 °C with a lifetime of approximately 35 min, Fig. S6 (ESI†). Such decomposition has been previously reported for CPPO in the CTAB micelle system.[23]

The remarkably efficient single-dye NIR-II CL observed herein encouraged us to pursue the underlying mechanism for low energy single-dye CL systems. A series of carefully designed dyes with the photon excitation energy from NIR-I

Table 1 The photo-properties of the investigated dyes in THF with 10% H_2O (ICG in MeOH as QY ref. 24)

Dyes	Abs_{Max} (nm)	Em_{Max} (nm)	EC (M^{-1} cm^{-1})	QY (%)	QY_{900} (%)	QY_{1000} (%)
Q842	825	842	170 000	4.03 ± 0.14	0.84	0.17
IR785	785	803	190 000	5.20 ± 0.45	0.58	0.10
Q995	958	995	145 000	0.26 ± 0.05	0.26	0.12
Q1044	1004	1044	89 000	0.064 ± 0.01	0.064	0.059
IR26	1079	1120	140 000	0.026 ± 0.005	0.026	0.026
Q1086	1057	1086	76 000	0.020 ± 0.005	0.020	0.020

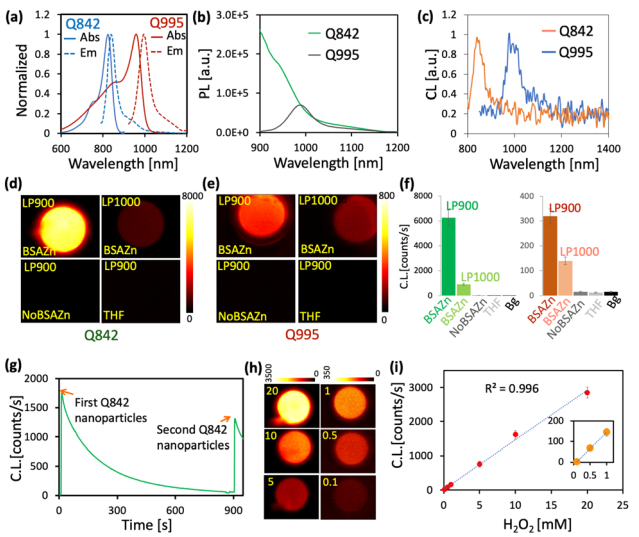

Fig. 1 (a) The PL and absorption spectra of Q995 and Q842 in THF (10% H_2O). (b) The PL spectra of Q995 and Q842 with the same absorbance at 785 nm. (c) The CL spectra of Q995 and Q842 in THF (10% H_2O). (d) The NIR-II CL image of the Q842 nanosystem. (e) The NIR-II CL image of the Q995 nanosystem. (f) The CL intensity of Q842 and Q995 at different experimental conditions as in (d) and (e). (g) The CL kinetics of the Q842 nanosystem. (h) The CL image of the Q842 nanosystem at variation of H_2O_2 concentration. (i) The CL of the Q842 nanosystem as a function of H_2O_2 concentration as in (g). All experiments were done with exposure time 1 s and details in Table S3 (ESI†).

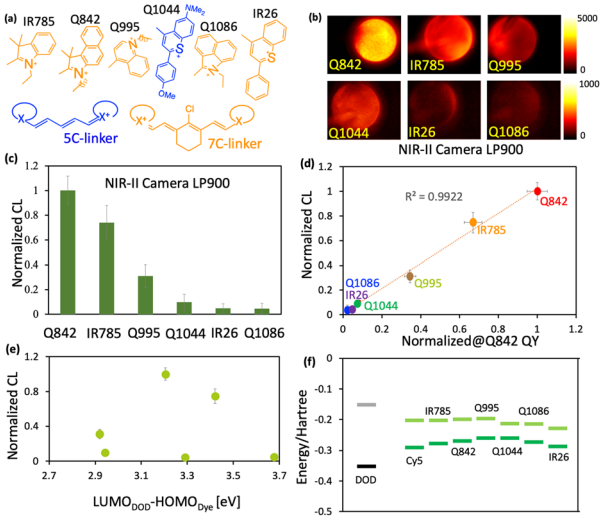

Fig. 2 Electronic properties and CL of the designed dyes. (a) The molecular structure of the investigated dyes. (b) The CL image of NIR dyes, with exposure time 1 s, NIR-II camera 900 nm long pass filter, dye concentration about 0.03 μmol ml^{-1}, and H_2O_2, 50 mM (v/v 10%). (c) The normalized CL of the investigated dyes. (d) The normalized CL as a function of the quantum yield of the investigated dyes. (e) The normalized CL as a function of the $LUMO_{DOD}$–$HOMO_{dye}$ energy gap. (f) The energy level of the HOMO and LUMO of the investigated dyes and DOD.

to NIR-II (785 nm to 1057 nm) are shown in Fig. 2(a), Fig. S8 (ESI†) and the corresponding absorption and PL spectra in Fig. S9 (ESI†). With richer electron density of heterocyclic groups and a longer polymethine linker, the corresponding electronic transition energy would be lower, Fig. S8, S9, ESI† and Table 1. Furthermore, a relatively broad shoulder absorption was observed for Q995 in THF with 10% H_2O, which well overlaps with the absorption of IR785 and Q842. On account of such broad absorption spectrum, Q995 was able to be taken as the fluorescence reference for both IR785 and Q842 at the excitation wavelength of about 785 nm and for Q1086, IR26, and Q1044 at excitation around 980 nm. This provides the right approach for direct comparison of the emission quantum yield in such an extended wavelength range from 800 nm to 1100 nm, Table 1. The intensity calibrated emission spectra of the investigated dyes beyond 900 nm are shown in Fig. S10 (ESI†) and the emission quantum yields (QYs) at different wavelength regions are shown in Table 1. For emission wavelengths above 1000 nm, the Q842 gives a higher QY than all other investigated dyes, about 0.17%. The total QY of Q995 was found to be about 10-fold higher than that of IR26.

Fig. 2(b) shows the CL image of the investigated dyes recorded *via* NIR-II camera in the THF solution. A bright CL was observed for the Q842, IR785, Q995 and Q1044. The CL image was conducted under the condition that CPPO is about 1 molar equivalent to dye avoiding multi-excitation of single dyes. Furthermore, 2.5 mM NaOH solution was applied to burst the CL.[25] The basic condition could accelerate the H_2O_2 dissociation and generate a large amount of DOD in a short time span.[25] Fig. 2(c) gives the relative CL intensity of the investigated dyes, normalized to that of Q842. A linear correlation between the emission QY of the investigated dyes and the CL intensity was established in the wavelength range beyond 900 nm, as shown in Fig. 2(d) and Fig. S13, S14 (ESI†). Nevertheless, we did not find any reasonable correlation for the CL intensity to the corresponding $LUMO_{DOD}$–$HOMO_{dye}$ energy gap, as shown in Fig. 2(e) and (f). This indicates that the CL of the investigated cyanine derivatives is dominated by the emission quantum yield rather than the $LUMO_{DOD}$–$HOMO_{dye}$ energy gap.

In viewing the HOMO and LUMO energy level of the designed cyanine dyes, we found a huge energy gap between the $HOMO_{dye}$ and $LUMO_{DOD}$, as shown in Fig. 3(a) and Table S1 (ESI†). Such an energy gap is even much higher than the direct electronic transition energy from $HOMO_{dye}$ to $LUMO_{dye}$. It might not be reasonable for the HOMO electron of dyes bypassing the $LUMO_{dye}$ to populate the $LUMO_{DOD}$. As a result, directly correlating the $LUMO_{DOD}$–$HOMO_{dye}$ energy gap with the CL efficiency might lack theoretical support. In order to investigate the electron transfer mechanism of such an efficient single-dye NIR-II CL system, the transition state (TS) along the DOD dissociation path was found, Fig. 3(b), and the geometry coordination in ESI.† The dissociated state (DOD@D) was taken with a largely elongated C–C bond. An interesting variation of the LUMO orbital energy was observed along the dissociation pathway of DOD, first descending significantly to the DOD@TS and then rising dramatically to DOD@D, Fig. 3(b). Nevertheless, there is no significant variation in the HOMO orbital energy. The LUMO orbital energy of the DOD@TS was found to be lower than the HOMO energy of all investigated dyes (Fig. 3(b)). On passing through the transition state, the LUMO orbital was lifted dramatically to even higher than the LUMO energy of the investigated dyes, as the LUMO of the DOD@D state, Fig. 3(b).

Fig. 3(c) illustrates the possible electron transfer mechanism of such an efficient single-dye NIR-II CL system. The HOMO electron of the dye may first transfer to a lowered LUMO orbital of a certain state around DOD@TS, and then pass through the transition state to gain energy. Eventually, an excited state of dye would be formed at a certain

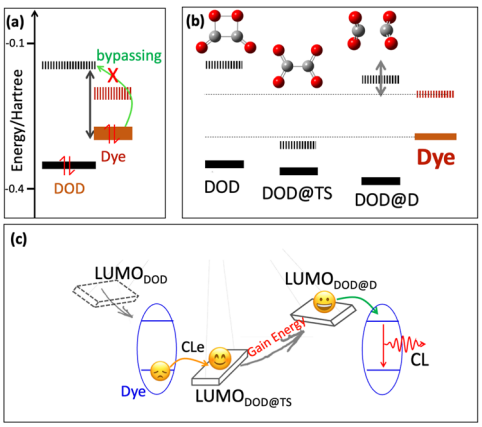

Fig. 3 Electronic properties of the CL system. (a) The relative HOMO and LUMO energy levels of the DOD and cyanine dyes. (b) The relative HOMO and LUMO energy levels of the DOD, DOD@TS (Transition State), DOD@D (Dissociated state) and cyanine dyes. (c) Orbital swing scheme for the electron transfer of the single-dye NIR-II CL system.

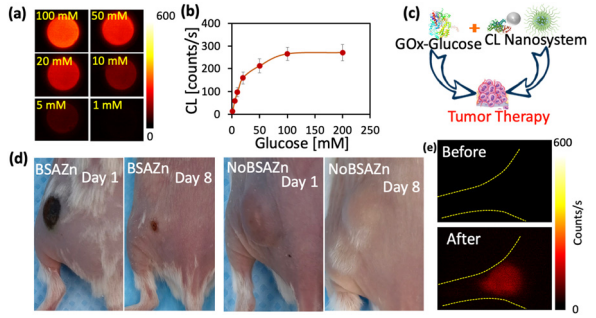

Fig. 4 The NIR-II CL nanosystem for *in vivo* application. (a) The CL image of the Q825 nanosystem in the presence of GOx at different glucose concentrations. (b) The CL intensity as a function of glucose concentration. (c) The scheme of the H_2O_2 tumor therapy *via* Gox-Glucose and the NIR-II CL nanosystem. (d) The image of the Gox-Glucose therapy effect for treating with and without BSAZn nanoenzyme. (e) The *in vivo* CL image of mouse left hind limb before and after injection of 10 μL 1 M H_2O_2, with exposure time 1 s. Experimental details are in Table S3 (ESI†).

point where the back electron transfer is favourable (from the LUMO of DOD@D to the LUMO of the dye). It is notable that during such electron transfer pathways, the electron always undergoes an exergonic process, instead of the endergonic pathway overcoming the large energy gap ($LUMO_{DOD}$–$HOMO_{dye}$) as usually considered.[13,14] Therefore, the electron transfer steps would not limit the NIR-II CL efficiency.

The excellent single-dye NIR-II CL nanosystem was demonstrated for certain biological applications as the glucose sensor, *in vivo* H_2O_2 imaging and cancer therapy, Fig. 4. It is well known that the glucose oxidase enzyme (GOx) is able to convert glucose into H_2O_2 in the presence of O_2.[26,27] The NIR-II CL intensity as a function of the glucose concentration was shown in Fig. 4(a) and (b). With increasing the concentration of glucose, the CL intensity was gradually increased. As the glucose concentration exceeds 100 mM, the NIR-II CL reached a plateau. The plateau region might indicate that the number of Gox enzymes limits the generation of H_2O_2. Despite the fact that H_2O_2 is one of the most energetic species, it is quite inert in comparison to the more reactive species, like $^{\bullet}OH$, $^1O_2$ and $^{\bullet}OOH$. As shown in Fig. 4(c) and (d), with the BSAZn nanoenzyme, the Gox-Glucose could introduce significant damage on the tumor tissue. A burn scar could be observed on the first day after administration, and the tumor almost shrunk away within 8 days. Furthermore, *in vivo* NIR-II CL was performed *via* subcutaneous injection of 1 M H_2O_2, Fig. 4(e). A clear CL could be observed after the injection of H_2O_2.

In summary, we carefully designed a series of cyanine dyes with excellent photo-properties, *via* which a bright single-dye NIR-II CL system was realized. Both theoretical and experimental evidence suggests that the electron transfer processes would not be the efficiency-limiting step for such a single-dye NIR-II CL system. Furthermore, a surprising enhancement was found for the BASZn nanoenzyme involved CL nanosystem by about three orders of magnitude. Such an efficient NIR-II CL nanosystem was demonstrated for *in vivo* H_2O_2 imaging and the sensing of glucose. The proposed electron transfer mechanism would provide a reasonable guideline for the design of novel single-dye NIR-II CL systems.

Q. S. conceived and designed the experiments. Z. C., C. L., and Q. S. performed the experiments. Q. S. and Z. C. analyzed the data and wrote the manuscript. Q. S., Z. C., C. L, X. Z., H. L., L. G., J. D. discussed the results and commented on the manuscript.

This work was supported by the National Natural Science Foundation of China (no. 22077135) and the Natural Science Foundation of Shenzhen (no. JCYJ20200109115633343).

Conflicts of interest

The authors declare no competing financial interest.

Notes and references

1 G. Hong, S. Diao, A. L. Antaris and H. Dai, *Chem. Rev.*, 2015, **115**(19), 10816–10906.
2 Z. Chang, F. Liu, L. Wang, M. Deng, C. Zhou, Q. Sun and J. Chu, *Chin. Chem. Lett.*, 2019, **30**(10), 1856–1882.
3 N. G. Horton, K. Wang, D. Kobat, C. G. Clark, F. W. Wise, C. B. Schaffer and C. Xu, *Nat. Photonics*, 2013, **7**(3), 205–209.
4 G. Hong, S. Diao, J. Chang, A. L. Antaris, C. Chen, B. Zhang, S. Zhao, D. N. Atochin, P. L. Huang, K. I. Andreasson, C. J. Kuo and H. Dai, *Nat. Photonics*, 2014, **8**(9), 723–730.
5 D. Lee, S. Khaja, J. C. Velasquez-Castano, C. Sun, J. Petros, W. R. Taylor and N. Murthy, *Nat. Mater.*, 2007, **6**(10), 765–769.
6 J. Huang, J. Li, Q. Miao and K. Pu, *Nat. Mater.*, 2019, **18**(10), 1133–1143.
7 H. W. Yeh, O. Karmach, A. Ji, D. Carter, M. M. Martins-Green and H. W. Ai, *Nat. Methods*, 2017, **14**(10), 971–974.
8 Y. Su, J. R. Walker, Y. Park, T. P. Smith, L. X. Liu, M. P. Hall, L. Labanieh, R. Hurst, D. C. Wang, L. P. Encell, N. Kim, F. Zhang, M. A. Kay, K. M. Casey, J. R. Cochran, C. L. Mackall, T. A. Kirkland and M. Z. Lin, *Nat. Methods*, 2020, **17**(8), 852–860.
9 M. P. Hall, C. C. Woodroofe, M. G. Wood, I. Que, M. Van'T Root, Y. Ridwan, C. Shi, T. A. Kirkland, L. P. Encell, K. V. Wood, C. Löwik and L. Mezzanotte, *Nat. Commun.*, 2018, **9**(1), 132.
10 A. M. Loening and S. S. Gambhir, *Nat. Methods*, 2007, **4**(8), 641–643.
11 M. Yang, J. Huang, J. Fan, J. Du, K. Pu and X. Peng, *Chem. Soc. Rev.*, 2020, **49**(19), 6800–6815.
12 A. J. Shuhendler, K. Pu, L. Cui, J. P. Uetrecht and J. Rao, *Nat. Biotechnol.*, 2014, **32**(4), 373–380.
13 X. Zhen, C. Zhang, K. L. Lim and K. Pu, *ACS Nano*, 2016, **10**(6), 6400–6409.
14 Y. D. Lee, C. K. Lim, A. Singh, J. Koh, J. Kim, I. C. Kwon and S. Kim, *ACS Nano*, 2012, **6**(8), 6759–6766.
15 Y. Yang, S. Wang, L. Lu, Q. Zhang, P. Yu, Y. Fan and F. Zhang, *Angew. Chem., Int. Ed.*, 2020, **59**(42), 18380–18385.
16 H. Shen, F. Sun, X. Zhu, J. Zhang, X. Ou, J. Zhang, C. Xu, H. H. Y. Sung, I. D. Williams, S. Chen, R. T. K. Kwok, J. W. Y. Lam, J. Sun, F. Zhang and B. Z. Tang, *J. Am. Chem. Soc.*, 2022, **144**, 15391–15402.
17 M. Vacher, I. Fdez Galván, B. W. Ding, S. Schramm, R. Berraud-Pache, P. Naumov, N. Ferré, I. Navizet, D. Roca-Sanjuán, W. J. Baader and R. Lindh, *Chem. Rev.*, 2018, **118**(15), 6927–6974.
18 T. Myochin, K. Kiyose, K. Hanaoka, H. Kojima, T. Terai and T. Nagano, *J. Am. Chem. Soc.*, 2011, **133**(10), 3401–3409.
19 Z. Lei, C. Sun, P. Pei, S. Wang, D. Li, X. Zhang and F. Zhang, *Angew. Chem., Int. Ed.*, 2019, **58**(24), 8166–8171.
20 R. Tian, Q. Zeng, S. Zhu, J. Lau, S. Chandra, R. Ertsey, K. S. Hettie, T. Teraphongphom, Z. Hu, G. Niu, D. O. Kiesewetter, H. Sun, X. Zhang, A. L. Antaris, B. R. Brooks and X. Chen, *Sci. Adv.*, 2019, **5**(9), eaaw0672.
21 R. B. Altman, D. S. Terry, Z. Zhou, Q. Zheng, P. Geggier, R. A. Kolster, Y. Zhao, J. D. Warren and S. C. Blanchard, *Nat. Methods*, 2012, **9**(1), 68–71.
22 (*a*) Z. Hu, C. Fang, B. Li, Z. Zhang, C. Cao, M. Cai, S. Su, X. Sun, X. Shi, C. Li, T. Zhou, Y. Zhang, C. Chi, P. He, X. Xia, Y. Chen, S. S. Gambhir, Z. Cheng and J. Tian, *Nat. Biomed. Eng.*, 2020, **4**, 259–271; (*b*) W. Zhou, Y. Cao, D. Sui and C. Lu, *Anal. Chem.*, 2016, **88**, 2659–2665; (*c*) C. Shen, Q. Lou, K. Liu, L. Dong and C. Shan, *Nano Today*, 2020, **35**, 100954.
23 T. S. Kuntzleman, K. Rohrer and E. Schultz, *J. Chem. Educ.*, 2012, **89**, 910–916.
24 N. S. James, Y. Chen, P. Joshi, T. Y. Ohulchanskyy, M. Henary, L. Strekowski and R. K. Pandey, *Theranostics*, 2013, **3**(9), 692–702.
25 L. Gao, J. Zhuang, L. Nie, J. Zhang, Y. Zhang, N. Gu, T. Wang, J. Feng, D. Yang, S. Perrett and X. Yan, *Nat. Nanotechnol.*, 2007, **2**(9), 577–583.
26 M. Xie, Z. Zhang, W. Guan, W. Zhou and C. Lu, *Anal. Chem.*, 2019, **91**(4), 2652–2658.
27 C. Wang, J. Yang, C. Dong and S. Shi, *Adv. Ther.*, 2020, **3**(10), 1–29.

